ORIGINAL PAPER

Kinetic relations and local energy balance for LEFM from a nonlocal peridynamic model

Prashant K. Jha(iD) · **Robert P. Lipton**(iD)

© Springer Nature B.V. 2020

Abstract A simple nonlocal field theory of peridynamic type is applied to model brittle fracture. The kinetic relation for the crack tip velocity given by Linear Elastic Fracture Mechanics (LEFM) is recovered directly from the nonlocal dynamics, this is seen both theoretically and in simulations. An explicit formula for the change of internal energy inside a neighborhood enclosing the crack tip is found for the nonlocal model and applied to LEFM.

1 Introduction

The fracture of solids can be viewed as a collective interaction across length scales. Application of sufficient stress or strain to a brittle material breaks atomistic bonds leading to fracture at macroscopic scales.

P. K. Jha
Oden Institute for Computational Engineering and Sciences, The University of Texas at Austin, Austin, TX 78712, USA e-mail: pjha@utexas.edu

R. P. Lipton (✉)
Department of Mathematics and Center for Computation and Technology, Louisiana State University, Baton Rouge, LA 70803, USA e-mail: lipton@lsu.edu

The appeal of a nonlocal fracture theory like peridynamics Silling (2000), Silling et al. (2007) is that fracture is captured as an emergent phenomenon. At the same time such a theory needs to recover the established theory of dynamic fracture mechanics described in Freund (1990), Ravi-Chandar (2004), Anderson (2005), Slepian (2002) as a limiting case. Motivated by these observations we consider a nonlocal peridynamic model (cohesive dynamics) proposed in Lipton (2014, 2016). The length scale of nonlocal interaction between any material point and its neighbors is called the *horizon*. Here the force strain relation between two points is linear elastic for small strains, softens under sufficiently large strain and ultimately becomes zero, see Fig. 2. In this nonlocal model displacement gradients can become steep and localize onto thin regions, see Jha and Lipton (2020). This model is used to show the kinetic relation for the velocity of the crack tip given by LEFM Freund (1990) follows in the limit of vanishing horizon.

In this paper the kinetic relation of LEFM is recovered from the nonlocal model in two different ways. The first approach to recovering the kinetic relation is to note that the same equation of motion applies everywhere in the body for the nonlocal model. We use this to show that local power balance is given by the stationarity in time of the internal energy of a small domain containing the crack tip. The change in internal energy is shown to be the difference between the elastic energy flowing into the crack and the kinetic energy

and stress work flux flowing into the domain, which is given by formula (18). To leading order the stress work flux is precisely the rate of energy needed to create new surface (21). These results are obtained directly and exclusively from the dynamics governed by the nonlocal Cauchy equations of motion for a continuum body. This is the explicit connection between the non-local Cauchy equations of motion derived from double well potentials and the energy rate required to make new surface. For remote boundary loading we apply energy balance and pass to the local limit to recover the celebrated kinetic relation for the modern theory of dynamic fracture mechanics articulated in Freund (1990), Ravi-Chandar (2004), Anderson (2005), Slepian (2002), see 4.1. Next it is shown that local power balance must hold for the nonlocal model when the displacement field is translation invariant inside a neighborhood of the crack (see Sect. 4.2). We pass to the limit of vanishing horizon to recover that the same holds true for LEFM. As a second approach we develop a nonlocal dynamic J integral and apply Mott's hypothesis on energy balance to a small region surrounding the crack tip. This is done in Sect. 4.3. The kinetic relation of LFEM is then obtained from the nonlocal model by passing the limit of vanishing nonlocality. Here it is pointed out that the approach of Sect. 4.1 is self contained and follows exclusively from the nonlocal Cauchy equation of motion. On the other hand the approach of Sect. 4.3 follows the classic one Freund (1990) and uses the nonlocal model to only compute the flow of elastic energy into the crack tip.

Next we provide a computational example to illustrate that power balance holds in the neighborhood of the crack tip using the nonlocal model. The fracture toughness $\mathcal{G}_c$, density, and elastic modulus of the material are prescribed. The numerical simulation using the nonlocal model is carried out for a single edge notch specimen of finite width and length. The simulation delivers a mode I crack traveling with constant velocity at roughly half of the Rayleigh wave speed. This simulation is consistent with the experimental results reported in Goldman et al. (2010). The change in internal energy inside a small neighborhood is calculated using (18) and is zero, i.e., power balance holds for a dynamic crack traveling at constant velocity V. The elastic energy flowing into a small neighborhood of the crack tip is $\mathcal{F}$ and the power balance inside a neighbor-hood of diameter δ is of the form

$$\mathcal{G}_c \approx \frac{\mathcal{F}}{V}. \tag{1}$$

Here $\approx$ indicates agreement to leading order in δ. This demonstrates that the energy released per unit length during crack growth at constant velocity is equal to the elastic energy flowing into the crack tip (see Sect. 5). It is important to note that the power balance (1) emerges through simulation and calculation using (18) as opposed to being independently postulated on physical grounds. In other words local power balance is a consequence of the nonlocal dynamics. The simulation and calculation are described in Sect. 5.

The paper is organized as follows: The nonlocal model of peridynamic type is presented in Sect. 2. Sect. 3 describes the fracture toughness and elastic properties associated with the nonlocal model. The main results given by the local energy balance and the recovery of the kinetic relation for LEFM are presented in 4. For clarity we postpone the derivations - calculations for later (see Sects. 6 and 7) and present simulations that emphasize the local energy balance in Sect. 5. Section 6 calculates the energy flow into the crack tip for the nonlocal model. Section 7 explicitly shows how the stress work flowing into the crack tip corresponds to the power required to create new fracture surface. The results are summarized in Sect. 8.
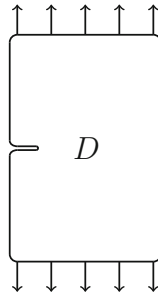
2 Nonlocal modeling

The appeal of nonlocal peridynamic models is that fracture appears as an emergent phenomena generated by the underlying field theory eliminating the need for supplemental kinetic relations describing crack growth. The deformation field inside the body for points x at time t is written $u(x, t)$. The peridynamic model is described simply by the balance of linear momentum of the form

$$\rho u_{tt}(x, t) = \int_{\mathcal{H}_\epsilon(x)} f(y, x) \, dy + b(x, t) \tag{2}$$

where $\mathcal{H}_\epsilon(x)$ is a neighborhood of x, ρ is the density, b is the body force density field, and f is a material-dependent constitutive law that represents the force density that a point y inside the neighborhood exerts on x as a result of the deformation field. The radius ϵ of the neighborhood is referred to as the *horizon*. Here all points satisfy the same basic field equations (2).

Fig. 1 Single-edge-notch

This approach to fracture modeling was introduced in Silling (2000) and Silling et al. (2007).

We work with a class of peridynamic models with nonlocal forces derived from double well potentials. See Lipton (2014), Lipton (2016). The term double well describes the force potential between two points. One of the wells is degenerate and appears at infinity while the other is at zero strain. For small strains the nonlocal force is linearly elastic but for larger strains the force begins to soften and then approaches zero after reaching a critical strain. The associated nonlocal dynamics is called *cohesive dynamics*. We consider a single edge notch specimen as given in Fig. 1 in plane stress.

In this treatment the displacement field $\boldsymbol{u} : D \times [0, T] \rightarrow \mathbb{R}^2$ is small compared to the size of the specimen D and the deformed configuration is the same as the reference configuration. We have $\boldsymbol{u} = \boldsymbol{u}(\boldsymbol{x}, t)$ as a function of space and time but will suppress the $\boldsymbol{x}$ dependence when convenient and write $\boldsymbol{u}(t)$. The tensile strain S between two points $\boldsymbol{x}, \boldsymbol{y}$ in D along the direction $\boldsymbol{e}_{\boldsymbol{y}-\boldsymbol{x}}$ is defined as

$$S(\boldsymbol{y}, \boldsymbol{x}, \boldsymbol{u}(t)) = \frac{\boldsymbol{u}(\boldsymbol{y}, t) - \boldsymbol{u}(\boldsymbol{x}, t)}{|\boldsymbol{y} - \boldsymbol{x}|} \cdot \boldsymbol{e}_{\boldsymbol{y}-\boldsymbol{x}}, \qquad (3)$$

where $\boldsymbol{e}_{\boldsymbol{y}-\boldsymbol{x}} = \frac{\boldsymbol{y}-\boldsymbol{x}}{|\boldsymbol{y}-\boldsymbol{x}|}$ is a unit vector and "·" is the dot product.

In the double well model the force acting between material points $\boldsymbol{x}$ and $\boldsymbol{y}$ is initially elastic and then softens and decays to zero as the strain between points increases, see Fig. 2. The critical strain $S_c > 0$ for which the force begins to soften is given by

$$S_c = \frac{r^c}{\sqrt{|\boldsymbol{y} - \boldsymbol{x}|}}, \qquad (4)$$

and S_+ is the strain at which the force goes to zero

$$S_+ = \frac{r^+}{\sqrt{|\boldsymbol{y} - \boldsymbol{x}|}}. \qquad (5)$$
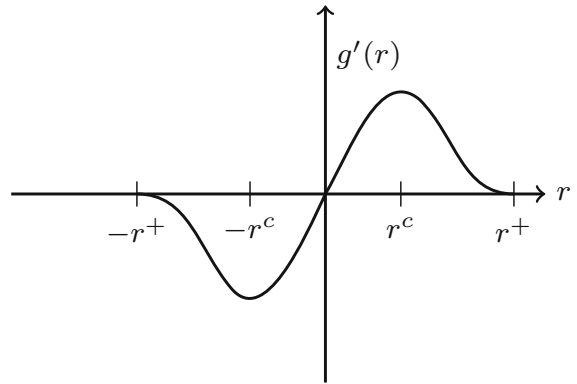
Fig. 2 Cohesive force. The force goes smoothly to zero at $\pm r^+$

The nonlocal force is defined in terms of a double well potential. The potential is a function of the strain and is defined for all $\boldsymbol{x}, \boldsymbol{y}$ in D by

$$\mathcal{W}^\epsilon(S(\boldsymbol{y}, \boldsymbol{x}, \boldsymbol{u}(t))) = J^\epsilon(|\boldsymbol{y} - \boldsymbol{x}|) \frac{1}{\epsilon^3 \omega_2 |\boldsymbol{y} - \boldsymbol{x}|}$$
$$g(\sqrt{|\boldsymbol{y} - \boldsymbol{x}|} S(\boldsymbol{y}, \boldsymbol{x}, \boldsymbol{u}(t))) \qquad (6)$$

where $\mathcal{W}^\epsilon(S(\boldsymbol{y}, \boldsymbol{x}, \boldsymbol{u}(t)))$ is the pairwise force potential per unit length between two points $\boldsymbol{x}$ and $\boldsymbol{y}$. It is described in terms of its potential function g, given by

$$g(r) = h(r^2) \qquad (7)$$

where h is concave. Here ω_2 is the area of the unit disk and $\epsilon^2 \omega_2$ is the area of the horizon $\mathcal{H}_\epsilon(\boldsymbol{x})$. The influence function $J^\epsilon(|\boldsymbol{y} - \boldsymbol{x}|)$ is a measure of the influence that the point $\boldsymbol{y}$ has on $\boldsymbol{x}$. Only points inside the horizon can influence $\boldsymbol{x}$ so $J^\epsilon(|\boldsymbol{y} - \boldsymbol{x}|)$ nonzero for $|\boldsymbol{y} - \boldsymbol{x}| < \epsilon$ and zero otherwise. We take J^ϵ to be of the form: $J^\epsilon(|\boldsymbol{y} - \boldsymbol{x}|) = J(\frac{|\boldsymbol{y}-\boldsymbol{x}|}{\epsilon})$ with $J(r) = 0$ for $r \geq 1$ and $0 \leq J(r) \leq M < \infty$ for $r < 1$.

The displacement field $\boldsymbol{u}(\boldsymbol{x}, t)$ evolves according to a nonlocal version of Cauchy's equations of motion for a continuum body
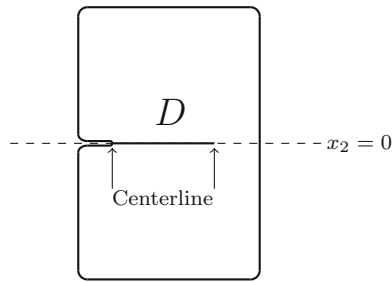
$$\rho \ddot{\boldsymbol{u}}^\epsilon(\boldsymbol{x}, t) = \mathcal{L}^\epsilon(\boldsymbol{u}^\epsilon)(\boldsymbol{x}, t) + \boldsymbol{b}(\boldsymbol{x}, t), \text{ for } \boldsymbol{x} \in D. \quad (8)$$

Here $\mathcal{L}^\epsilon(\boldsymbol{u}^\epsilon)$ is

$$\mathcal{L}^\epsilon(\boldsymbol{u}^\epsilon) = \int_{\mathcal{H}_\epsilon(\boldsymbol{x})} \boldsymbol{f}^\epsilon(\boldsymbol{y}, \boldsymbol{x}) \, d\boldsymbol{y} \qquad (9)$$

and $\boldsymbol{f}^\epsilon(\boldsymbol{x}, \boldsymbol{y})$ is given by

$$\boldsymbol{f}^\epsilon(\boldsymbol{x}, \boldsymbol{y})$$
$$= 2\partial_S \mathcal{W}^\epsilon(S(\boldsymbol{y}, \boldsymbol{x}, \boldsymbol{u}^\epsilon(t))) \boldsymbol{e}_{\boldsymbol{y}-\boldsymbol{x}}, \qquad (10)$$

Fig. 3 Failure zone centerline

where

$$\partial_S \mathcal{W}^\epsilon(S(\boldsymbol{y}, \boldsymbol{x}, \boldsymbol{u}^\epsilon(t)))$$
$$= \frac{1}{\epsilon^3 \omega_2} \frac{J^\epsilon(|\boldsymbol{y} - \boldsymbol{x}|)}{|\boldsymbol{y} - \boldsymbol{x}|} \partial_S g(\sqrt{|\boldsymbol{y} - \boldsymbol{x}|} S(\boldsymbol{y}, \boldsymbol{x}, \boldsymbol{u}^\epsilon(t))). \tag{11}$$

The dynamics is complemented with the initial data

$$\boldsymbol{u}^\epsilon(\boldsymbol{x}, 0) = \boldsymbol{u}_0(\boldsymbol{x}), \qquad \partial_t \boldsymbol{u}^\epsilon(\boldsymbol{x}, 0) = \boldsymbol{v}_0(\boldsymbol{x}), \tag{12}$$

and the appropriate traction and Dirichlet boundary conditions described in Sect. 5.

2.1 Failure Zone - Process Zone

The failure zone represents the crack in the nonlocal model. It is characterized by the failure zone centerline. The failure zone centerline starts at the notch and propagates into the interior of the specimen. The force between two points $\boldsymbol{x}$ and $\boldsymbol{y}$ separated by the failure zone centerline is zero. The centerline is shown in Fig. 3 and the failure zone is the grey region in Fig. 4. For the boundary conditions chosen here failure is in tension and confined to a neighborhood of the $x_2 = 0$ axis of width 2ϵ. Just in front of the failure zone is the process zone where the force between two points $\boldsymbol{x}$ and $\boldsymbol{y}$ on either side of the $x_2 = 0$ axis is decreasing with increasing strain. At the leading edge of the crack one sees force softening between points $\boldsymbol{x}$ and $\boldsymbol{y}$ and as the crack centerline moves forward passing between $\boldsymbol{x}$ and $\boldsymbol{y}$ the force between $\boldsymbol{x}$ and $\boldsymbol{y}$ decreases to zero, see Fig. 4. It needs to be stressed the failure zone and process zone emerge from the nonlocal dynamics and are not prescribed. For example see Sect. 5, Fig. 10.

3 Fracture toughness and elastic properties for the cohesive model: as specified through the force potential

For finite horizon $\epsilon > 0$ the fracture toughness and elastic moduli are recovered directly from the cohesive strain potential $\mathcal{W}^\epsilon(S(\boldsymbol{y}, \boldsymbol{x}, \boldsymbol{u}(t)))$. Here the fracture toughness $\mathcal{G}_c$ is defined to be the energy per unit length required eliminate force between each point $\boldsymbol{x}$ and $\boldsymbol{y}$ on either side of a line in $\mathbb{R}^2$. In this case the line is the $x_2 = 0$ axis. Because of the finite length scale of interaction only the force between pairs of points within an ϵ distance from the line are considered. The fracture toughness $\mathcal{G}_c$ is calculated in Lipton (2016). Proceeding as in Silling and Askari (2005) we have

$$\mathcal{G}_c = 2 \int_0^\epsilon \int_z^\epsilon \int_0^{\arccos(z/\zeta)} \mathcal{W}^\epsilon(\mathcal{S}_+) \zeta^2 \, d\psi \, d\zeta \, dz \tag{13}$$

where $\zeta = |\boldsymbol{y} - \boldsymbol{x}|$, see Fig. 5. Substitution of $\mathcal{W}^\epsilon(S(\boldsymbol{y}, \boldsymbol{x}, \boldsymbol{u}(t)))$ given by (6) into (13) delivers

$$\mathcal{G}_c = \frac{4}{\pi} \int_0^1 h(S_+^2) r^2 J(r) dr. \tag{14}$$

It is evident from this calculation that the fracture toughness is the same for all choice of horizons. This provides the rational behind the ϵ scaling of the potential (6) for the cohesive model. Moreover the layer width on either side of the crack centerline over which the force is applied to create new surface tends to zero with ϵ. In this way ϵ can be interpreted as a parameter associated with the size of the failure zone of the material. Equation (14) gives a way to calibrate the function h that specifies the potential (7) when $\mathcal{G}_c$ is given.

Further calibration of h is possible using the elastic moduli of the material. To calibrate h we relate elastic moduli of the material to the cohesive potential $\mathcal{W}^\epsilon(S(\boldsymbol{y}, \boldsymbol{x}, \boldsymbol{u}(t)))$. When the horizon is sufficiently small we suppose the displacement inside $\mathcal{H}_\epsilon(\boldsymbol{x})$ is affine, that is, $\boldsymbol{u}(\boldsymbol{x}) = F\boldsymbol{x}$ where F is a constant matrix. For small strains, i.e., $\mathcal{S} = Fe \cdot e \ll \mathcal{S}_c$, a Taylor series expansion at zero strain shows that the strain potential is linear elastic to leading order and characterized by elastic moduli μ and λ associated with a linear elastic isotropic material

$$W(\boldsymbol{x}) = \int_{\mathcal{H}_\epsilon(\boldsymbol{x})} |\boldsymbol{y} - \boldsymbol{x}| \mathcal{W}^\epsilon(S(\boldsymbol{y}, \boldsymbol{x}, \boldsymbol{u})) \, d\boldsymbol{y}$$
$$= \mu |F|^2 + \frac{\lambda}{2} |Tr\{F\}|^2 + O(\epsilon |F|^4). \tag{15}$$

Fig. 4 The failure zone is
the grey shaded region and
the process zone is the clear
region inside the contour
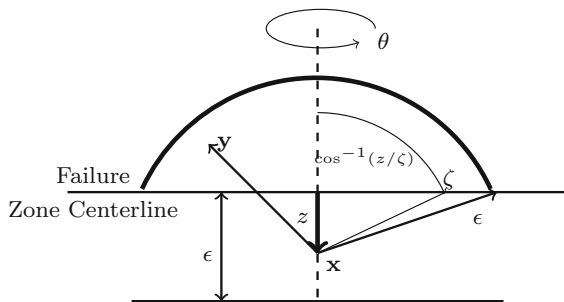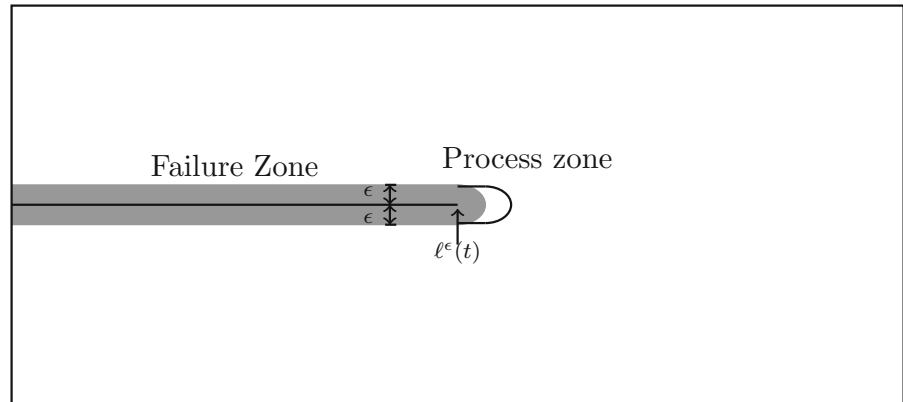
Fig. 5 Evaluation of fracture toughness $\mathcal{G}_c$. For each point $\boldsymbol{x}$ along the dashed line, $0 \leq z \leq \epsilon$, the work required to break the interaction between $\boldsymbol{x}$ and $\boldsymbol{y}$ in the spherical cap is summed up in (13) using spherical coordinates centered at $\boldsymbol{x}$. This summation is done on both sides of the failure zone centerline

The elastic moduli λ and μ are calculated directly from the strain energy density and are given by

$$\mu = \lambda = M \frac{1}{4} h'(0) , \qquad (16)$$

where the constant $M = \int_0^1 r^2 J(r) dr$. The elasticity tensor is given by

$$\mathbb{C}_{ijkl} = 2\mu \left(\frac{\delta_{ik}\delta_{jl} + \delta_{il}\delta_{jk}}{2} \right) + \lambda \delta_{ij}\delta_{kl}. \qquad (17)$$

When μ is specified $h'(0)$ is determined by (16). For the simple potentials considered here the elasticity corresponds to materials with Poisson's ratio 1/4, i.e., $\lambda = \mu$. It is noted that we are free to consider other multi well potentials and general choices of Poisson's ratios Jha and Lipton (2019b); these correspond to state based peridynamic models Silling et al. (2007).

4 Kinetic relation from nonlocal dynamics

In this section we show that the well known kinetic relation for the velocity of the crack tip, Freund (1990), follows from the nonlocal model in the limit of vanishing *horizon* in two different ways. We begin by defining the kinetic energy density by $T^\epsilon = \rho |\dot{\boldsymbol{u}}^\epsilon(\boldsymbol{x}, t)|^2/2$ and the stress work density for the nonlocal model given by $W^\epsilon(\boldsymbol{x}) = \int_{\mathcal{H}_\epsilon(\boldsymbol{x})} |\boldsymbol{y} - \boldsymbol{x}| \mathcal{W}^\epsilon(S(\boldsymbol{y}, \boldsymbol{x}, \boldsymbol{u}^\epsilon(t))) \, d\boldsymbol{y}$.

4.1 Rate of internal energy change inside a domain containing the crack tip

Note that for the nonlocal model the same equation applies everywhere in the body. Because of this we can calculate the time rate of change of internal energy of a domain containing the crack tip and pass to the limit of local interactions. Fix a contour Γ_δ of diameter δ surrounding the domain $\mathcal{P}_\delta(t)$ containing the tip of the failure zone for the local model, see Fig. 6. Recall that the line centered within the failure zone running from the notch to the leading edge of the failure zone is called the failure zone center line, see Fig. 3. We investigate power balance in regions containing the tip of the failure zone. We suppose $\mathcal{P}_\delta(t)$ is moving with the crack tip velocity $V^\epsilon(t)$ along the horizontal axis. A direct calculation given in Sect. 6 establishes the following explicit formula for the rate of change in internal energy inside the domain containing the edge of the failure zone.

Rate of change of internal energy for a region containing the crack tip for the nonlocal model:

$$\frac{d}{dt} \int_{\mathcal{P}_\delta(t)} T^\epsilon + W^\epsilon \, d\boldsymbol{x} = I^\epsilon(\Gamma_\delta(t)) \qquad (18)$$
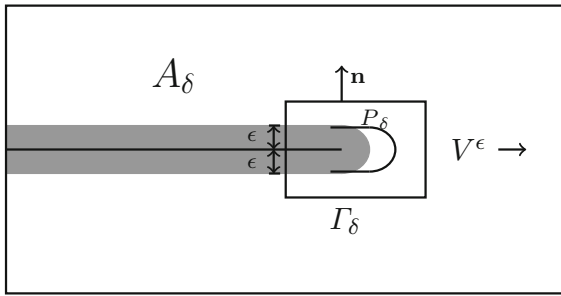
Fig. 6 Contour Γ_δ surrounding the domain P_δ moving with the velocity V^ϵ of the failure zone in grey and process zone

with

$$I^\epsilon(\Gamma_\delta(t)) = \int_{\Gamma_\delta(t)} (T^\epsilon + W^\epsilon) V^\epsilon \boldsymbol{e}^1 \cdot \boldsymbol{n} \, ds - E^\epsilon(\Gamma_\delta(t)),$$

(19)

where $\boldsymbol{n}$ is the outward directed unit normal, ds is an element of arc length, and $\boldsymbol{e}^1$ is the unit vector pointing in the direction of crack propagation. The rate of elastic energy flowing into the domain surrounding the crack tip is

$$E^\epsilon(\Gamma_\delta(t))$$
$$= \int_{A_\delta(t)} \int_{\mathcal{H}_\epsilon(\boldsymbol{x}) \cap \mathcal{P}_\delta(t)} \partial_S \mathcal{W}^\epsilon(S(\boldsymbol{y}, \boldsymbol{x}, \boldsymbol{u}^\epsilon)) \boldsymbol{e}_{\boldsymbol{y}-\boldsymbol{x}} \quad (20)$$
$$\cdot (\dot{\boldsymbol{u}}^\epsilon(\boldsymbol{x}) + \dot{\boldsymbol{u}}^\epsilon(\boldsymbol{y})) \, d\boldsymbol{y} d\boldsymbol{x},$$

where $A_\delta(t)$ is the part of D exterior to $\mathcal{P}_\delta(t)$. These relations follow directly from the nonlocal Cauchy's equations of motion (8), this is shown in Sect. 6. Equation (18) gives the following energy criterion for local power balance:

Local power balance of a neighborhood containing the crack tip is given by the stationarity of its internal energy with respect to time.

The stress work density flowing into the moving domain is related to fracture toughness by

$$\int_{\Gamma_\delta(t)} W^\epsilon V^\epsilon \boldsymbol{e}^1 \cdot \boldsymbol{n} \, ds = -\mathcal{G}_c V^\epsilon(t) + O(\delta).$$

(21)

and

$$\int_{\Gamma_\delta(t)} T^\epsilon V^\epsilon \boldsymbol{e}^1 \cdot \boldsymbol{n} \, ds = O(\delta).$$

(22)

These identities are obtained in Sect. 7. One recalls that the stress power is that part of the externally supplied power which is not converted into kinetic energy. This is corroborated by the numerical experiments provided in Sect. 5.

When the horizon goes to zero we get for $V^\epsilon \boldsymbol{e}^1 \to V \boldsymbol{e}^1$,

$$\lim_{\epsilon \to 0} \int_{\Gamma_\delta(t)} W^\epsilon V^\epsilon \boldsymbol{e}^1 \cdot \boldsymbol{n} \, ds = -\mathcal{G}_c V(t),$$
$$\lim_{\epsilon \to 0} E^\epsilon(\Gamma_\delta(t)) = -\int_{\Gamma_\delta} \mathbb{C}\mathcal{E}\boldsymbol{u}^0 \boldsymbol{n} \cdot \dot{\boldsymbol{u}}^0 \, ds + O(\delta),$$

(23)

where $\mathbb{C}\mathcal{E}\boldsymbol{u}^0 \boldsymbol{n} \cdot \dot{\boldsymbol{u}}^0$ is the energy flux into P_δ. The change in internal energy inside the domain containing the crack tip is given by:

$$\lim_{\epsilon \to 0} \frac{d}{dt} \int_{\mathcal{P}_\delta(t)} T^\epsilon + W^\epsilon \, d\boldsymbol{x}$$
$$= \int_{\Gamma_\delta} \mathbb{C}\mathcal{E}\boldsymbol{u}^0 \boldsymbol{n} \cdot \dot{\boldsymbol{u}}^0 \, ds - \mathcal{G}_c V(t) + O(\delta).$$

(24)

Off the crack the displacement $\boldsymbol{u}^0$ satisfies Cauchy's equations of motion for a continuum body

$$\rho \ddot{\boldsymbol{u}}^0 = div\left(\mathbb{C}\mathcal{E}\boldsymbol{u}^0\right) + \boldsymbol{b}$$

(25)

where $\mathcal{E}_{ij} = 1/2(\boldsymbol{u}^0_{i,j} + \boldsymbol{u}^0_{j,i})$ is the symmetrized gradient Lipton (2014, 2016). The crack flanks are traction free and $\boldsymbol{u}^0$ satisfies boundary and initial conditions see Lipton and Jha (2020).

For $\mathcal{F} = \lim_{\delta \to 0} \int_{\Gamma_\delta} \mathbb{C}\mathcal{E}\boldsymbol{u}^0 \boldsymbol{n} \cdot \dot{\boldsymbol{u}}^0 \, ds$ we get

$$\lim_{\delta \to 0} \lim_{\epsilon \to 0} \frac{d}{dt} \int_{\mathcal{P}_\delta(t)} T^\epsilon + W^\epsilon \, d\boldsymbol{x} + \mathcal{G}_c V = \mathcal{F}.$$

(26)

Power balance gives

$$\lim_{\delta \to 0} \lim_{\epsilon \to 0} \frac{d}{dt} \int_{\mathcal{P}_\delta(t)} T^\epsilon + W^\epsilon \, d\boldsymbol{x} = 0,$$

(27)

and from Atkinson and Eshelby (1965), Kostrov and Nikitin (1970), Freund (1972), and Willis (1975) the semi explicit kinetic relation connecting the energy flux into the crack tip to the crack velocity follows from (26) and is of the form given by Freund and Clifton (1974)

$$\mathcal{G}_c = \frac{\mathcal{F}}{V} = \frac{1 + \nu}{E} \frac{V^2}{c_s^2 D} \alpha_t K_I^2(t),$$

(28)

were ν is the Poisson's ratio, E is the Young modulus V is the crack velocity, c_s is the shear wave speed, $c_l = (\lambda + 2\mu/\rho)^{1/2}$ is the longitudinal wave speed, $D = 4\alpha_s \alpha_l - (1 + \alpha_s^2)^2$, and $\alpha_s = (1 - V^2/c_s^2)^{1/2}$, $\alpha_l = (1 - V^2/c_l^2)^{1/2}$. Here $K_I(t)$ is the mode I dynamic stress intensity factor and depends on the details of the loading and is not explicit.

In summary (24) and (26) are recovered directly from (8) and are a consequence of the nonlocal dynamics in the $\epsilon = 0$ limit. The recovery is possible since the nonlocal model is well defined over *the failure zone*. The rate of change in energy (18) and its limit (24) are calculated in Sects. 6 and 7.
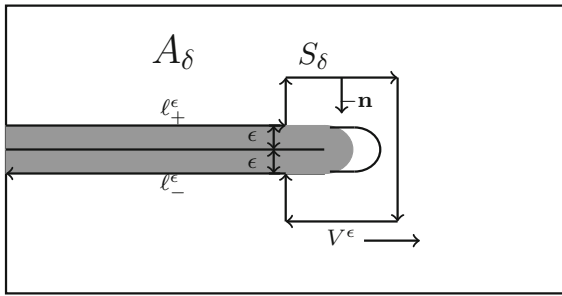
Fig. 7 The contour S_δ surrounding the tip of the failure zone (in gray) and process zone moving with velocity V^ϵ

4.2 Local power balance for translation invariant displacement in the neighborhood of the crack tip.

In this section we consider a constant velocity crack for our peridynamic model and suppose that the displacement is translation invariant in the neighborhood of the crack tip. These assumptions are standard in LEFM Rice (1968b), Sih (1968), Irwin (1967), Freund and Clifton (1974), Nillison (1974). For this case we show that the change in the internal energy of the neighborhood surrounding the crack tip is zero. So energy balance holds for the peridynamic model. To see this consider the translation invariant displacement field of the form $\boldsymbol{u}^\epsilon(\boldsymbol{x}, t) = \boldsymbol{u}^\epsilon(\boldsymbol{x} - t V \boldsymbol{e}^1)$ where t is time and V is the constant crack speed directed along the positive x_1 axis. It follows that the stress power and rate of change in kinetic energy inside $\mathcal{P}_\delta$ are given by

$$\dot{W}^\epsilon = -\partial_{x_1} W^\epsilon V$$
$$\dot{T}^\epsilon = -\partial_{x_1} T^\epsilon V. \qquad (29)$$

So from the divergence theorem we get

$$\int_{\mathcal{P}_\delta(t)} \dot{T}^\epsilon + \dot{W}^\epsilon \, d\boldsymbol{x}$$
$$= -\int_{\Gamma_\delta(t)} (T^\epsilon + W^\epsilon) V^\epsilon \boldsymbol{e}^1 \cdot \boldsymbol{n} \, ds, \qquad (30)$$

and by Reynolds transport theorem (54) we discover the nonlocal model gives local power balance, i.e.,

$$\frac{d}{dt} \int_{\mathcal{P}_\delta(t)} T^\epsilon + W^\epsilon \, d\boldsymbol{x} = 0. \qquad (31)$$

From this together with (18), (30) we conclude that

$$\int_{\Gamma_\delta(t)} (T^\epsilon + W^\epsilon) V^\epsilon \boldsymbol{e}^1 \cdot \boldsymbol{n} \, ds - E^\epsilon(\Gamma_\delta(t)) = 0, \quad (32)$$

and from (21) our peridynamic model gives

$$\mathcal{G}_c V = -E^\epsilon(\Gamma_\delta(t)) + O(\delta). \qquad (33)$$

On passing to the zero horizon limit in the nonlocal dynamics we see that local power balance for constant velocity cracks modeled by LEFM is given by

Local power balance for LEFM:

$$\mathcal{G}_c V = \lim_{\delta \to 0} \int_{\Gamma_\delta} \mathbb{C}\mathcal{E}\boldsymbol{u}^0 \boldsymbol{n} \cdot \dot{\boldsymbol{u}}^0 \, ds. \qquad (34)$$

The local power balance for LEFM has been predicted here using the nonlocal model.

4.3 The peridynamic J integral and Linear Elastic Fracture Mechanics

For LEFM the elastic field near the crack tip is derived from the local Cauchy's equations of motion for a continuum body. This gives the flow of elastic energy into the crack tip, Freund (1990). On the other hand the kinetic relation for LEFM does not follow from the local Cauchy's equation of motion alone. Instead the kinetic relation for LEFM follows from Mott's hypothesis Mott (1948) on the balance of elastic energy flowing into the crack tip and power needed to create new fracture surface Freund (1990). In this section we will proceed like is done in the local theory but obtain the J integral for the nonlocal model and compare with the previous results. We compute the time rate of change of the internal energy of the domain $A_\delta(t)$ surrounding the crack tip inside the contour shown in Fig. 7. Calculation as in Sect. 7 shows that the energy flux from A_δ into the flanks of the failure zone $\ell_\pm^\epsilon$ is zero so the energy flux through the surface S_δ of diameter δ is the energy flow into the tip of the damage zone given by $J^\epsilon(S_\delta(t))$ where

$$J^\epsilon(S_\delta(t)) = -\int_{S_\delta(t)} (T^\epsilon + W^\epsilon) V^\epsilon \boldsymbol{e}^1 \cdot \boldsymbol{n} \, ds \qquad (35)$$
$$+ E^\epsilon(S_\delta(t)),$$

here **n** is the outward directed unit normal. The rate of elastic energy flowing into in the domain surrounding the crack tip is

$$E^\epsilon(S_\delta(t))$$
$$= \int_{A_\delta(t)} \int_{\mathcal{H}_\epsilon(\boldsymbol{x}) \cap \mathcal{Q}_\delta(t)} \partial_S \mathcal{W}^\epsilon(S(\boldsymbol{y}, \boldsymbol{x}, \boldsymbol{u}^\epsilon)) \boldsymbol{e}_{\boldsymbol{y}-\boldsymbol{x}} \quad (36)$$
$$\cdot (\dot{\boldsymbol{u}}^\epsilon(\boldsymbol{x}) + \dot{\boldsymbol{u}}^\epsilon(\boldsymbol{y})) \, d\boldsymbol{y} d\boldsymbol{x}.$$

When the horizon goes to zero a calculation as in Sect. 7 shows,

$$\lim_{\epsilon \to 0} \int_{S_\delta(t)} (T^\epsilon + W^\epsilon) V^\epsilon \boldsymbol{e}^1 \cdot \boldsymbol{n} \, ds = O(\delta),$$
$$\lim_{\epsilon \to 0} E^\epsilon(S_\delta(t)) = -\int_{S_\delta} \mathbb{C}\mathcal{E}\boldsymbol{u}^0 \boldsymbol{n} \cdot \dot{\boldsymbol{u}}^0 \, ds, \tag{37}$$

and the local limit of the peridynamic J integral is given by

$$J(S_\delta(t)) = -\int_{S_\delta} \mathbb{C}\mathcal{E}\boldsymbol{u}^0 \boldsymbol{n} \cdot \dot{\boldsymbol{u}}^0 \, ds + O(\delta) \tag{38}$$

and on taking $\delta = 0$ we recover the total energy flux into the crack tip as in LEFM. Note that (38) differs from (24) since S_δ does not cross the failure zone. Formula (38) is the well known J integral of LEFM introduced in Rice (1968a), and developed for dynamics Atkinson and Eshelby (1965), Freund (1972), and Sih (1970). Applying energy balance and using the general form of the elastic fields near the crack tip for samples of infinite extent Atkinson and Eshelby (1965), Kostrov and Nikitin (1970), Freund (1972), and Willis (1975) we recover the crack tip kinetic relation (28).

Alternate versions of the peridynamic J integral have been deduced for dynamic fracture problems in Silling and Lehoucq (2010) using balance laws. For quasi-static fracture problems the work of Hu et al. (2012), derive a J integral using an infinitesimal virtual crack extension and Stenström and Eriksson (2019) accelerate the numerical calculation of the J integral using the peridynamic displacement field. The dynamic J integral developed here is derived from the equation of motion using integration by parts and naturally agrees with Silling and Lehoucq (2010). However the explicit form is different and follows from a suitable change of variables. In addition the "crack" for the nonlocal model is not artificially assumed infinitesimally thin as in other approaches but instead we use the fact that it has a thickness that is twice the peridynamic horizon.

To summarize the approach of Sect. 4.1 is self contained and follows exclusively from the nonlocal Cauchy equation of motion. While the approach of Sect. 4.3 reflects the classic approach and uses the nonlocal model to compute the elastic energy only. It is then equated to the energy required to create new fracture surface invoking Mott's hypothesis as is done with the local theory.

5 Numerical simulation and analysis

The principal point of peridynamic modeling is that crack motion is part of the solution and emerge from the nonlocal dynamics. This is the hallmark of peridynamic modeling Silling (2000), Ha and Bobaru (2010). In this section, we provide a numerical simulation using the cohesive dynamics given by (8) to see that a crack moving at constant speed satisfies energy balance. The numerical computation also shows that the stress work flux is nearly equal to the energy release rate as anticipated by the theory, see (21), (22), (23).

5.1 Setup

We consider a sample of material with Young's modulus $E = 88$ kPa, Poisson's ratio $\nu = 0.25$, and material density $\rho = 1011.2$ kg/m^3. The Rayleigh wave speed and shear wave speed for the sample are $c_R = 5.502$ m/s and $c_s = 5.9$ m/s respectively. The numerical simulation is motivated by the experiments carried out in Goldman et al. (2010) and the material domain, horizon, discretization, and boundary conditions are shown in Fig. 8. In this work we assume plane stress conditions. We consider a pre-cracked specimen as shown in Fig. 8. The pre-crack is of length $l = 3$ mm. The critical energy release rate is taken to be $\mathcal{G}_c = 20$ J/m^2.

The force potential is $g(r) = c(1 - \exp[-\beta r^2])$, where c, β are constants. The influence function is of the form $J(r) = 1 - r$. Equations (14), (16) are used to calibrate the values of the parameters c, β. For the material properties listed above we get $c = 15.705$, $\beta = 8965.378$. We define the damage $Z(\boldsymbol{x})$ at a material point $\boldsymbol{x}$ as follows:

$$Z(\boldsymbol{x}) = \sup_{\boldsymbol{y} \in \mathcal{H}_\epsilon(\boldsymbol{x})} \frac{|S(\boldsymbol{y}, \boldsymbol{x}, \boldsymbol{u}(t))|}{S_c(\boldsymbol{y}, \boldsymbol{x})}. \tag{39}$$

A value $Z > 1$ implies that there are neighboring points $\boldsymbol{y}$ for which the bond-strain between points $\boldsymbol{y}$ and $\boldsymbol{x}$ lies above the critical strain.

We consider a uniform discretization and offset the crack vertically by $h/100$ where $h = 0.125$ mm is the mesh size so that the crack line is not on the grid line. For temporal discretization, we consider velocity-verlet scheme with time step size $\Delta t = 2.2 \, \mu$s and final time $T = 1.1$ s. For mesh convergence, we rely on our earlier work Jha and Lipton (2019b) where a similar

Fig. 8 Setup for steady state crack propagation experiment. Here $\epsilon = 0.75$ mm and $v = 1.475$ mm/s. Domain is uniformly discretized with mesh size $h = \epsilon/6 = 0.125$ mm
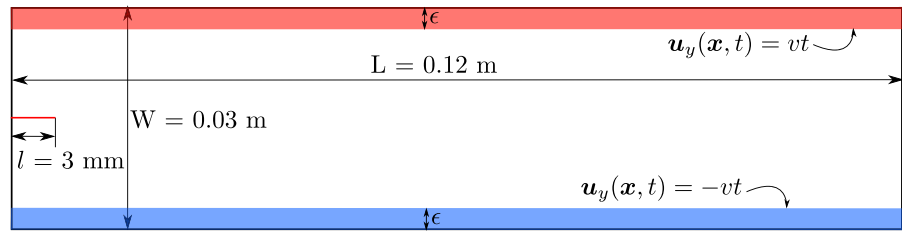
setup was considered and convergence with respect to the mesh was shown. To see if the simulation changes when using an unstructured mesh, we ran the same problem on unstructured mesh consisting of linear triangle elements. We first obtained the mesh using Gmsh library and then computed the nodal volume associated to each vertex in the mesh. Pairs of vertices and volumes form the particle mesh. The results were similar to the case of uniform discretization.

We choose crack tip location as a measure of convergence of the temporal discretization. Here the crack tip is recovered as a post processing step. In order to find the crack tip at any given time step we search the simulation output data for vertices with damage Z greater than 1 and the crack tip is the vertex such that

– No other vertex on the right side of the selected vertex exists with $Z > 1$.

To illustrate time convergence, we consider the same simulation but using a smaller time step $\Delta t = 1.1\,\mu s$. The crack tip position is compared for the two different time steps at times $t = 0.9603, 0.9647, 0.9801$ s. Here the x-coordinates of the crack tip for $\Delta t = 2.2\,\mu s$ and $\Delta t = 1.1\,\mu s$ are given by 0.011057, 0.02456, 0.072951 m and 0.011018, 0.024525, 0.072939 m respectively. The simulation for the time step $\Delta t = 2.2$ is shown in Fig. 9 at times $t = 0.9603, 0.9647, 0.9801$ s.

Crack velocities are computed over a longer time step $\overline{\Delta t}$, i.e. *Crack velocity = Distance traveled over timestep/$\overline{\Delta t}$*. Here $\overline{\Delta t} = 0.0022$s while the time step used in the simulation is $\Delta t = 2.2\,\mu s$. The choice of $\overline{\Delta t}$ smooths out the high frequency velocity fluctuations due to bond breaking and delivers an averaged crack velocity over an interval of length $\overline{\Delta t}$.

When labeling plots we will apply the following notation:

$$WV := \int_{\Gamma_\delta} W^\epsilon V^\epsilon \cdot n \, ds,$$

$$F_{pd} := -E^\epsilon(\Gamma_\delta)$$

$$\dot{E} := \frac{d}{dt} \int_{\mathcal{P}_\delta} T^\epsilon + W^\epsilon \, dx, \tag{40}$$

where V^ϵ is the crack velocity. All plotted quantities are in units of Joules/s. We will also display the total fracture energy at time t, denoted by PE, see (41), and the total energy released by a crack of length l, given by $GE = l \times \mathcal{G}_c$.

5.2 Results

The plot of crack velocity and deformation field surrounding the crack tip centerline at three selected times are shown in Fig. 9. Damage in the reference configuration is plotted in Fig. 10. The figure shows that damage is localized and corresponds to the crack in the nonlocal model and is of width $2(\epsilon + h)$. The crack velocity history given by Fig. 9 is in qualitative agreement with experimental results (Goldman et al. 2010, Figure 2). There is an initial increase in crack speed, but as waves reflect back from the boundary onto the crack tip the velocity becomes roughly constant. To display the crack opening displacement and the deformation of the specimen we have added the displacement field at the node to its nodal location. This is done for all nodal points in the specimen, see Fig. 9.

Next, we focus on regime of near constant crack speed corresponding to the time interval $[0.9647, 0.9801]$. As predicted from theory, see (21), $-WV$ agrees with $V\mathcal{G}_c$ see Fig. 11. The simulation also shows that the time rate of change in kinetic energy near the crack tip is small and F_{pd} is close to $V\mathcal{G}_c$ see Fig. 11. The bottom Fig. in 11 shows that the rate of total energy $\dot{E}$ in the constant crack speed regime is close to zero.

We compute the peridynamic energy of the failure zone and compare it with the classic fracture energy. For a crack of length at time t given by $l(t)$, the classic fracture energy (GE) is $GE(t) = G_c \times l(t)$. Recall the failure zone at time t is denoted by
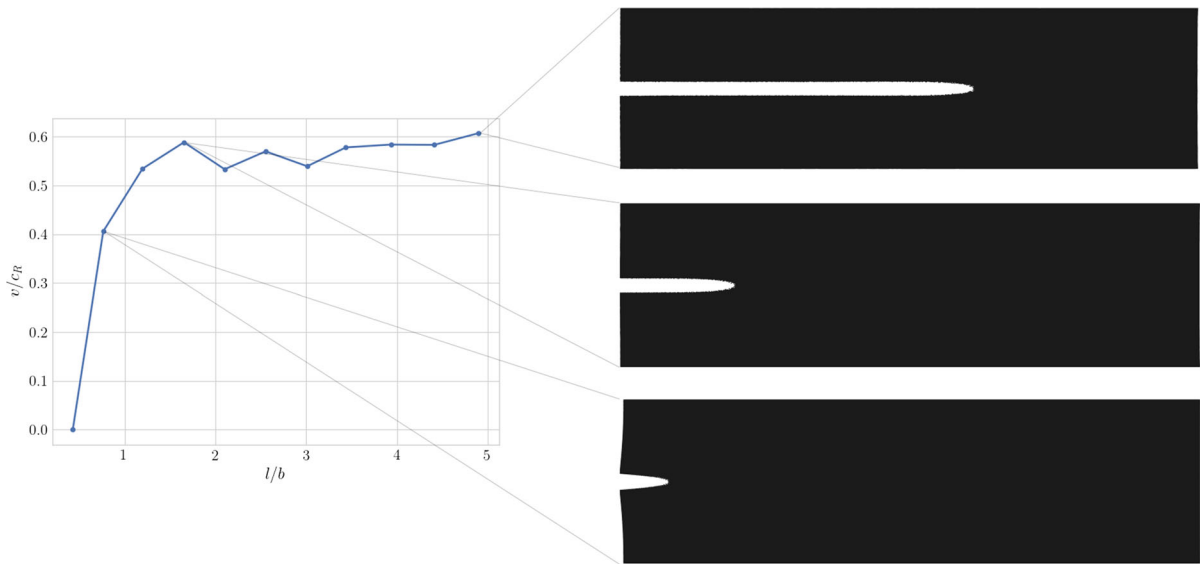
Fig. 9 Left: Crack velocity vs crack length. $b = 0.015$ m is the half width of the domain. $c_R = 5.502$ m/s is the Rayleigh wave speed. The crack velocity approaches steady state value of 0.6 which is consistent with the experimental result in Goldman et al. (2010); Bouchbinder et al. (2014). This is due to the fact that crack feels the boundary and wave reflection from the boundary obstructs crack to acquire more velocity. Right: Crack opening displacement and deformation in the specimen at times $t = 0.9603, 0.9647, 0.9801$ s
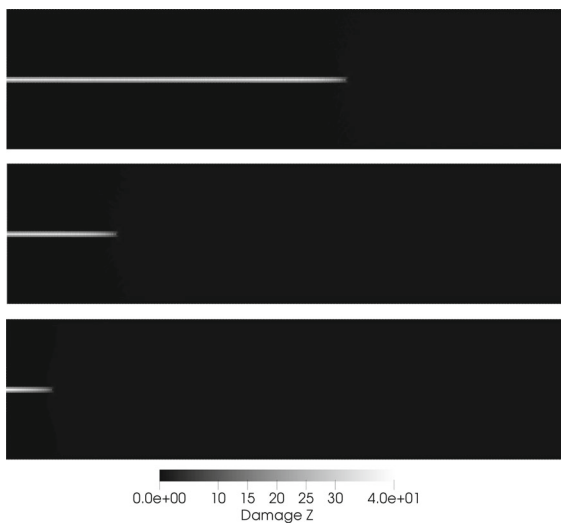
Fig. 10 The crack together with process zone is given for $Z > 1$ in the reference configuration at times $t = 0.9603, 0.9647, 0.9801$ s. Here the points where $Z > 1$ are shaded white all other points are shaded black. The crack is a thin region of thickness $2(\epsilon + h)$

$FZ^\epsilon(t)$ and the peridynamic fracture energy (PE) is given by

$$PE(t)$$
$$= \int_{FZ^\epsilon(t)} \left[\frac{1}{\epsilon^d \omega_d} \int_{H_\epsilon(x)} |y - x| \mathcal{W}^\epsilon(S(y, x, u)) \, dy \right] dx. \tag{41}$$

The peridynamic fracture energy is compared to the classic fracture energy in Fig. 12 and is seen to be nearly identical.

6 Change in internal energy on subdomains containing the crack tip for the nonlocal model

In this section we recover the rate of change of internal energy (18) using the nonlocal version of Cauchy's equations of motion for a continuum body given by (8). Consider the rectangular contour $\Gamma_\delta(t)$ of diameter δ bordering the domain $\mathcal{P}_\delta(t)$ containing the crack tip. We suppose $\mathcal{P}_\delta(t)$ is moving with the crack tip speed $V^\epsilon(t)$ see Fig. 6. It will be shown that the rate of change of energy inside $\mathcal{P}_\delta(t)$ for the nonlocal dynamics is given by (18). We start by introducing a nonlocal divergence theorem applied to the case at hand. To expedite taking $\epsilon \to 0$ limits in the next section we make the change of variables $y = x + \epsilon \xi$ where ξ

Fig. 11 Top: Normalized rate of energies given by F_{pd}, $-WV$ and LEFM rate $V \times \mathcal{G}_c$. Bottom: Negative of rate of total contour energy, $-\dot{E}$. Here energy rates are divided by $c_S\mathcal{G}_c$, where $c_s = 5.9m/s$ is the shear wave speed and $\mathcal{G}_c = 20.0J/m^2$ is the critical energy release rate. Plots are at time steps in the constant crack speed time interval [0.9647, 0.9801]. In both plots, the limits in y-axis are taken as [−0.1, 1.0] where the upper limit is the normalized energy rate associated to crack moving at shear wave speed
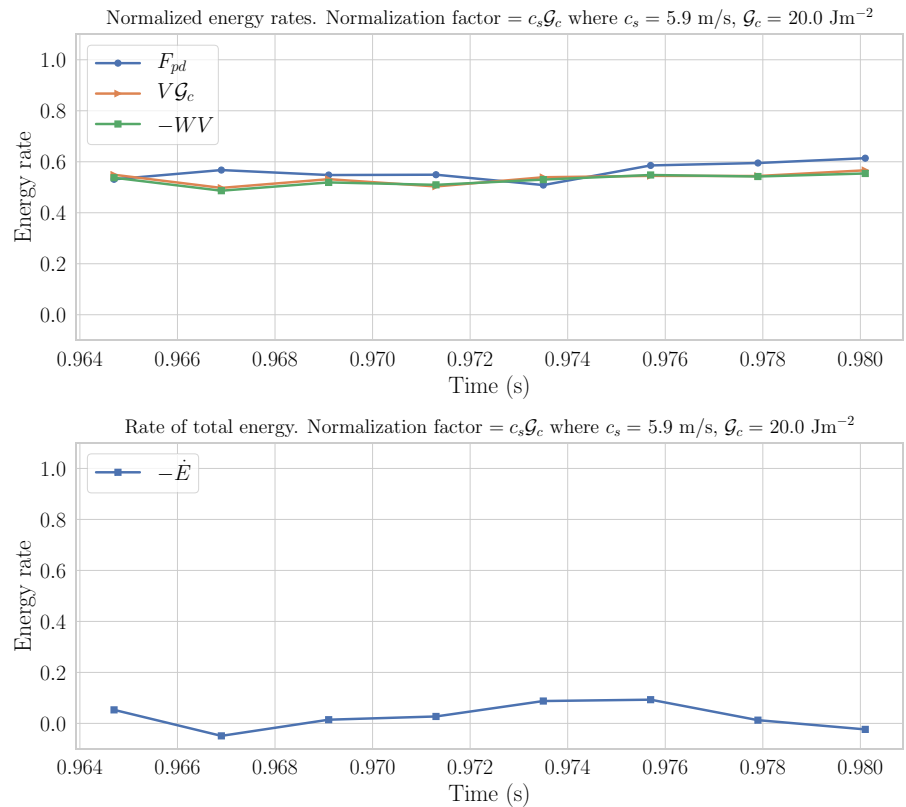
belongs to the unit disk at the origin $\mathcal{H}_1(0) = \{|\xi| < 1\}$ and $e = \xi/|\xi|$. The strain is written

$$\frac{u^\epsilon(x + \epsilon\xi) - u^\epsilon(x)}{\epsilon|\xi|}$$
$$:= D_e^{\epsilon|\xi|}u^\epsilon, \text{ and} \tag{42}$$
$$S(y, x, u^\epsilon(t)) = D_e^{\epsilon|\xi|}u^\epsilon \cdot e,$$

and the work done in straining the material between points y and x given by $|y - x|\partial_S\mathcal{W}^\epsilon(S(y, x, u^\epsilon(t)))$ transforms in the new variables to

$$\epsilon|\xi|\partial_S\mathcal{W}^\epsilon(D_e^{\epsilon|\xi|}u^\epsilon \cdot e)$$
$$= \frac{2|\xi|J(|\xi|)}{\epsilon^2\omega_2}h'(\epsilon|\xi||D_e^{\epsilon|\xi|}u^\epsilon \cdot e|^2)D_e^{\epsilon|\xi|}u^\epsilon \cdot e. \tag{43}$$

We will use the following nonlocal divergence theorem.
    Nonlocal divergence theorem:

$$\epsilon^2\int_{P_\delta(t)}\int_{\mathcal{H}_1(0)} D_{-e}^{\epsilon|\xi|}\left[\epsilon|\xi|\partial_S\mathcal{W}^\epsilon(D_e^{\epsilon|\xi|}u^\epsilon \cdot e)w(x) \cdot e\right]d\xi dx$$
$$= \epsilon^2\int_{\mathcal{H}_1(0)}\int_{(P_\delta(t)-\epsilon\xi)\setminus P_\delta(t)} \partial_S\mathcal{W}^\epsilon(D_e^{\epsilon|\xi|}u^\epsilon \cdot e)w(x) \cdot e\, dx d\xi$$
$$- \epsilon^2\int_{\mathcal{H}_1(0)}\int_{P_\delta(t)\setminus(P_\delta(t)-\epsilon\xi)} \partial_S\mathcal{W}^\epsilon(D_e^{\epsilon|\xi|}u^\epsilon \cdot e)w(x) \cdot e\, dx d\xi.$$
$$\tag{44}$$

This identity follows on applying the definition of $D_{-e}^{\epsilon|\xi|}\varphi = (\varphi(x - \epsilon\xi) - \varphi(x))/\epsilon|\xi|$ for scalar fields φ and Fubini's theorem. When convenient we set $A_\delta(t) = D \setminus P_\delta(t)$ and rewrite the last two terms of (44) in x and y variables to get

$$\epsilon^2\int_{P_\delta(t)}\int_{\mathcal{H}_1(0)} D_{-e}^{\epsilon|\xi|}\left[\epsilon|\xi|\partial_S\mathcal{W}^\epsilon(D_e^{\epsilon|\xi|}u^\epsilon \cdot e)w \cdot e\right]d\xi dx$$
$$= \int_{A_\delta(t)}\int_{\mathcal{H}_\epsilon(x)\cap P_\delta(t)} \partial_S\mathcal{W}^\epsilon(S(y, x, u^\epsilon(t)))(w(x) \tag{45}$$
$$+ w(y)) \cdot e_{y-x}\, dy dx,$$

and we can rewrite (45) in x and ξ variables to get

$$\epsilon^2\int_{P_\delta(t)}\int_{\mathcal{H}_1(0)} D_{-e}^{\epsilon|\xi|}\left[\epsilon|\xi|\partial_S\mathcal{W}^\epsilon(D_e^{\epsilon|\xi|}u^\epsilon \cdot e)w \cdot e\right]d\xi dx$$
$$= \epsilon^2\int_{\mathcal{H}_1(0)}\int_{(P_\delta(t)-\epsilon\xi)\setminus P_\delta(t)} \partial_S\mathcal{W}^\epsilon(D_e^{\epsilon|\xi|}u^\epsilon \cdot e)(w(x) \tag{46}$$
$$+ w(x + \epsilon\xi)) \cdot e\, dx d\xi.$$

Lastly a straight forward manipulation in (46) delivers the product rule:

Product rule

$$\epsilon^2 \int_{P_\delta(t)} \int_{\mathcal{H}_1(0)} D^{\epsilon|\xi|}_{-e} \left[\epsilon|\xi| \partial_S \mathcal{W}^\epsilon (D^{\epsilon|\xi|}_e \boldsymbol{u}^\epsilon \cdot \boldsymbol{e}) \boldsymbol{w}(\boldsymbol{x}) \cdot \boldsymbol{e} \right] d\xi d\boldsymbol{x}$$

$$= -\epsilon^2 \int_{P_\delta(t)} \int_{\mathcal{H}_1(0)} 2\partial_S \mathcal{W}^\epsilon (D^{\epsilon|\xi|}_e \boldsymbol{u}^\epsilon \cdot \boldsymbol{e}) \boldsymbol{e} \cdot \boldsymbol{w}(\boldsymbol{x}) \, d\xi d\boldsymbol{x} \quad (47)$$

$$- \epsilon^2 \int_{P_\delta(t)} \int_{\mathcal{H}_1(0)} \epsilon|\xi| \partial_S \mathcal{W}^\epsilon (D^{\epsilon|\xi|}_e \boldsymbol{u}^\epsilon \cdot \boldsymbol{e}) D^{\epsilon|\xi|}_e \boldsymbol{w} \cdot \boldsymbol{e} \, d\xi d\boldsymbol{x}.$$

We now recover (18) from (8). Multiplying both sides of (8) by $\dot{\boldsymbol{u}}^\epsilon$, integration over $P_\delta(t)$, and applying the product rule gives

$$\int_{P_\delta(t)} \partial_t \frac{\rho|\dot{\boldsymbol{u}}^\epsilon|^2}{2} \, d\boldsymbol{x}$$

$$= \epsilon^2 \int_{P_\delta(t)} \int_{\mathcal{H}_1(0)} 2\partial_S \mathcal{W}^\epsilon (D^{\epsilon|\xi|}_e \boldsymbol{u}^\epsilon \cdot \boldsymbol{e}) \dot{\boldsymbol{u}}^\epsilon(\boldsymbol{x}) \cdot \boldsymbol{e} \, d\xi d\boldsymbol{x}$$

$$= -\epsilon^2 \int_{P_\delta(t)} \int_{\mathcal{H}_1(0)} D^{\epsilon|\xi|}_{-e} \left[\epsilon|\xi| \partial_S \mathcal{W}^\epsilon (D^{\epsilon|\xi|}_e \boldsymbol{u}^\epsilon \cdot \boldsymbol{e}) \dot{\boldsymbol{u}}^\epsilon(\boldsymbol{x}) \cdot \boldsymbol{e} \right] d\xi d\boldsymbol{x} \quad (48)$$

$$- \epsilon^2 \int_{P_\delta(t)} \int_{\mathcal{H}_1(0)} \epsilon|\xi| \partial_S \mathcal{W}^\epsilon (D^{\epsilon|\xi|}_e \boldsymbol{u}^\epsilon \cdot \boldsymbol{e}) D^{\epsilon|\xi|}_e \dot{\boldsymbol{u}}^\epsilon \cdot \boldsymbol{e} \, d\xi d\boldsymbol{x}$$

Define the stress work density

$$W^\epsilon(\boldsymbol{x}, t) = \epsilon^2 \int_{\mathcal{H}_1(0)} \epsilon|\xi| \mathcal{W}^\epsilon (D^{\epsilon_n|\xi|}_e \boldsymbol{u}^\epsilon \cdot \boldsymbol{e}) \, d\xi. \quad (49)$$

We observe that the change in stress work density with respect to time (stress power density) is given by

$$\dot{W}^\epsilon = \int_{\mathcal{H}_1(0)} \epsilon^3 |\xi| \partial_S \mathcal{W}^\epsilon (D^{\epsilon|\xi|}_e \boldsymbol{u}^\epsilon \cdot \boldsymbol{e}) D^{\epsilon|\xi|}_e \dot{\boldsymbol{u}}^\epsilon \cdot \boldsymbol{e} \, d\xi, \quad (50)$$

and (48) becomes

$$\int_{P_\delta(t)} \dot{T}^\epsilon + \dot{W}^\epsilon \, d\boldsymbol{x}$$

$$= -\int_{P_\delta(t)} \int_{\mathcal{H}_1(0)} \epsilon^2 D^{\epsilon|\xi|}_{-e} \left[\epsilon|\xi| \partial_S \mathcal{W}^\epsilon (D^{\epsilon|\xi|}_e \boldsymbol{u}^\epsilon \cdot \boldsymbol{e}) \dot{\boldsymbol{u}}^\epsilon \cdot \boldsymbol{e} \right] d\xi d\boldsymbol{x}, \quad (51)$$

where $\dot{T}^\epsilon = \partial_t(\rho|\dot{\boldsymbol{u}}^\epsilon|^2/2)$.

Proceeding as in Freund (1990) and Willis (1975) we find the change of internal energy of $P_\delta(t)$. We consider the region R given by the tube in space time swept out by $P_\delta(t)$ moving with constant velocity V^ϵ in the x_1 direction. Here we consider the time interval $t_1 < t < t_2$. We write

$$\int_{t_1}^{t_2} \int_{P_\delta(t)} \partial_t(T^\epsilon + W^\epsilon) \, d\boldsymbol{x} \, dt$$

$$= \int_R \partial_t(T^\epsilon + W^\epsilon) \, d\boldsymbol{x} \, dt \quad (52)$$

$$= \int_{\partial R} (T^\epsilon + W^\epsilon) \frac{dt}{d\nu} \, d\mathcal{S},$$

where we have applied the divergence theorem and $\frac{dt}{d\nu}$ is the direction cosine of the exterior normal to R in the time direction and $d\mathcal{S}$ is the element of surface area.

We will parameterize the surface area element on the sides of ∂R as $d\mathcal{S} = \sqrt{1 + (V^\epsilon)^2} ds \, dt$ and on the sides

$$\frac{dt}{d\nu} = -\frac{V^\epsilon \boldsymbol{e}^1 \cdot \boldsymbol{n}}{\sqrt{1 + (V^\epsilon)^2}}$$

where $\boldsymbol{n}$ is the outward directed unit normal to $\partial P_\delta(t)$. Applying this to (52) gives the identity

$$\int_{t_1}^{t_2} \int_{P_\delta(t)} \partial_t(T^\epsilon + W^\epsilon) \, d\boldsymbol{x} \, dt$$

$$= -\int_{t_1}^{t_2} \int_{\partial P_\delta(t)} (T^\epsilon + W^\epsilon) \boldsymbol{e}^1 \cdot \boldsymbol{n} V^\epsilon \, ds \, dt \quad (53)$$

$$+ \int_{P_\delta(t_2)} T^\epsilon + W^\epsilon \, d\boldsymbol{x} - \int_{P_\delta(t_1)} T^\epsilon + W^\epsilon \, d\boldsymbol{x},$$

where the last two integrals are on the top and bottom faces of R at $t = t_2$ and t_1 respectively. Now take $t_1 = t$ and $t_2 = t + \Delta t$ divide by Δt and send $\Delta t \to 0$ in (53) to get the identity

$$\int_{P_\delta(t)} \partial_t(T^\epsilon + W^\epsilon) \, d\boldsymbol{x} = \frac{d}{dt} \int_{P_\delta(t)} T^\epsilon + W^\epsilon \, d\boldsymbol{x}$$

$$- \int_{\partial P_\delta(t)} (T^\epsilon + W^\epsilon) V^\epsilon \boldsymbol{e}^1 \cdot \boldsymbol{n} \, ds. \quad (54)$$

This is equivalent to using Reynolds transport theorem but it is obtained in a way that **does not require** $\dot{\boldsymbol{u}}^\epsilon$ to be differentiable in space. So (54) together with (51) and (45) deliver the change in internal energy:

$$\frac{d}{dt} \int_{P_\delta(t)} T^\epsilon + W^\epsilon \, d\boldsymbol{x}$$

$$= \int_{\partial P_\delta(t)} (T^\epsilon + W^\epsilon) V^\epsilon \boldsymbol{e}^1 \cdot \boldsymbol{n} \, ds \quad (55)$$

$$- \int_{A_\delta(t)} \int_{\mathcal{H}_\epsilon(\boldsymbol{x}) \cap P_\delta(t)} \partial_S \mathcal{W}^\epsilon (S(\boldsymbol{y}, \boldsymbol{x}, \boldsymbol{u}^\epsilon(t))) \boldsymbol{e}_{\boldsymbol{y} - \boldsymbol{x}}$$

$$\cdot (\dot{\boldsymbol{u}}^\epsilon(\boldsymbol{x}) + \dot{\boldsymbol{u}}^\epsilon(\boldsymbol{y})) \, d\boldsymbol{y} d\boldsymbol{x}$$

and (18) follows.

7 Formulas for peridynamic stress work and convergence of peridynamic stress work and elastic energy flux to those of the local model

In this section we establish (23). We start by discovering the crucial identities (21) and (22). We denote the four sides of the rectangular contour Γ_δ by Γ_i, $i = 1, \ldots, 4$ in Fig. 13. There is no contribution of the integrand to the integral on the lefthand side of (22) on

Peridynamic and classical fracture energy
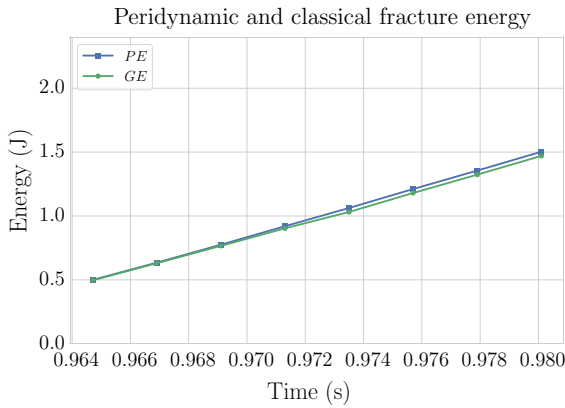
Fig. 12 Peridynamic and classical fracture energy. The interval along the y-axis is $[0, \mathcal{G}_c L]$, where L is the length of domain and is the maximum crack length

the sides 2 and 4 since $e^1 \cdot n = 0$ there. On side 3 the potential and kinetic energy densities are bounded so

$$\left| \int_{\Gamma_3} (T^\epsilon + W^\epsilon) V^\epsilon e^1 \cdot n \, ds \right| = O(\delta). \tag{56}$$

On side 1 we partition the contour Γ_1 into three parts. The first part is given by all points on Γ_1 that are further than ϵ away from $x_2 = 0$ call this $\Gamma_{1,+}$ and as before

$$\left| \int_{\Gamma_{1,+}} (T^\epsilon + W^\epsilon) V^\epsilon e^1 \cdot n \, ds \right| = O(\delta). \tag{57}$$

The part of Γ_1 with $0 \le x_2 \le \epsilon$ is denoted Γ_1^+ and the part with $-\epsilon \le x_2 < 0$ is denoted Γ_1^- and

$$\left| \int_{\Gamma_1^\pm} T^\epsilon V^\epsilon e^1 \cdot n \, ds \right| = O(\delta). \tag{58}$$

Now we calculate

$$\int_{\Gamma_1^+} W^\epsilon V^\epsilon e^1 \cdot n \, ds$$
$$= -V^\epsilon \int_{\Gamma_1^+} W^\epsilon \, ds$$
$$= -V^\epsilon \int_{\Gamma_1^+} \int_{\mathcal{H}_\epsilon(x) \cap K_\epsilon^+} |y - x| \mathcal{W}^\epsilon(S(y, x, u^\epsilon(t))) \, dy \, ds \tag{59}$$
$$- V^\epsilon \int_{\Gamma_1^+} \int_{\mathcal{H}_\epsilon(x) \cap K_\epsilon^-} |y - x| \mathcal{W}^\epsilon(S(y, x, u^\epsilon(t))) \, dy \, ds$$

Here $\mathcal{H}_\epsilon(x) \cap K_\epsilon^+$ is the subset of y in $\mathcal{H}_\epsilon(x)$ for which the vector with end points y and x crosses the failure zone centerline and $\mathcal{H}_\epsilon(x) \cap K_\epsilon^-$ is the subset of y in $\mathcal{H}_\epsilon(x)$ for which the vector with end points y and x does not cross the failure zone centerline. Calculation

Fig. 13 The sides of the contour Γ_δ is denoted by Γ_1 through Γ_4
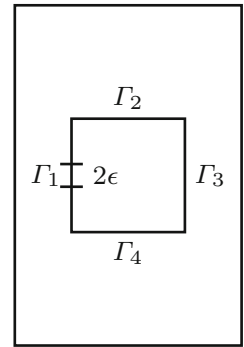
as in Sect. 3 gives

$$\int_{\Gamma_1^+} \int_{\mathcal{H}_\epsilon(x) \cap K_\epsilon^+} |y - x| \mathcal{W}^\epsilon(S(y, x, u^\epsilon(t))) \, dy \, ds$$
$$= \int_0^\epsilon \int_z^\epsilon \int_0^{\arccos(z/\zeta)} \mathcal{W}^\epsilon(\mathcal{S}_+) \zeta^2 \, d\psi \, d\zeta \, dz \tag{60}$$
$$= \frac{\mathcal{G}_c}{2},$$

and it follows from calculating as in (15) we get that

$$\left| \int_{\Gamma_1^+} \int_{\mathcal{H}_\epsilon(x) \cap K_\epsilon^-} |y - x| \mathcal{W}^\epsilon(S(y, x, u^{\epsilon n}(t))) \, dy \, ds \right| = O(\delta). \tag{61}$$

From (60) and (61) we conclude that

$$\int_{\Gamma_1^+} W^\epsilon V^\epsilon e^1 \cdot n \, ds = -V^\epsilon \int_{\Gamma_1^+} W^\epsilon \, ds$$
$$= -V^\epsilon \frac{\mathcal{G}_c}{2} + O(\delta). \tag{62}$$

An identical calculation shows

$$\int_{\Gamma_1^-} W^\epsilon V^\epsilon e^1 \cdot n \, ds = -V^\epsilon \frac{\mathcal{G}_c}{2} + O(\delta). \tag{63}$$

and (21) and (22) follow.

To conclude we show

$$\lim_{\epsilon \to 0} E^\epsilon(\Gamma_\delta(t)) = -\int_{\Gamma_\delta} \mathbb{C}\mathcal{E}u^0 n \cdot \dot{u}^0 \, ds. \tag{64}$$

Setting $\Delta_{\epsilon\xi}\dot{u}^\epsilon(x) = \dot{u}^\epsilon(x) + \dot{u}^\epsilon(x + \epsilon\xi)$ we have

$$E^\epsilon(\Gamma_\delta(t))$$
$$= \epsilon^2 \int_{P_\delta(t)} \int_{\mathcal{H}_1(0)} D_{-e}^{\epsilon|\xi|}$$
$$\left[\epsilon|\xi| \partial_S \mathcal{W}^\epsilon(D_e^{\epsilon|\xi|} u^\epsilon \cdot e) \dot{u}^\epsilon \cdot e \right] \, d\xi \, dx \tag{65}$$
$$= \epsilon^2 \int_{\mathcal{H}_1(0)} \int_{(P_\delta(t) - \epsilon\xi) \setminus P_\delta(t)} \partial_S \mathcal{W}^\epsilon(D_e^{\epsilon|\xi|} u^\epsilon \cdot e)$$
$$\Delta_{\epsilon\xi} \dot{u}^\epsilon(x) \cdot e \, dx \, d\xi.$$

Integration in the ξ variable is over the unit disc centered at the origin $\mathcal{H}_1(0)$. We split the unit disk into its for quadrants Q_i, $i = 1, \ldots, 4$. The boundary Γ_δ is the union of its four sides Γ_j, $j = 1, \ldots, 4$. Here the left and right sides are Γ_1 and Γ_3 respectively and the top and bottom sides are Γ_2 and Γ_4 respectively, see Fig. 14. We choose $\boldsymbol{n}$ to be the outward pointing normal vector to P_δ, $\boldsymbol{t}$ is the tangent vector to the boundary Γ_δ and points in the clockwise direction, and $\boldsymbol{e} = \xi/|\xi|$. For ξ in Q_1 the set of points $\boldsymbol{x} \in (P_\delta(t) - \epsilon\xi) \setminus P_\delta(t)$ is parameterized as $\boldsymbol{x} = \boldsymbol{t}x + \boldsymbol{n}(\epsilon|\xi|\boldsymbol{e} \cdot \boldsymbol{n})r$. Here x lies on $\Gamma_1 \cup \Gamma_4$ and $0 < r < 1$ and the area element is $-(\epsilon|\xi|\boldsymbol{e} \cdot \boldsymbol{n})dxdr$. For ξ in Q_2 the set of points $\boldsymbol{x} \in (P_\delta(t) - \epsilon\xi) \setminus P_\delta(t)$ is again parameterized as $\boldsymbol{x} = \boldsymbol{t}x + \boldsymbol{n}(\epsilon|\xi|\boldsymbol{e}\cdot\boldsymbol{n})r$ where x lies on $\Gamma_3\cup\Gamma_4$ and $0 < r < 1$ and the area element is given by the same formula. For ξ in Q_3 we have the same formula for the area element and parameterization and x lies on $\Gamma_3\cup\Gamma_4$ with $0 < r < 1$. Finally for ξ in Q_4 we have again the same formula for the area element and parameterization and x lies on $\Gamma_1\cup\Gamma_2$ with $0 < r < 1$. This parameterization and a change in order of integration delivers the formula for $E^\epsilon(\Gamma_\delta(t))$ given by

$$E^\epsilon(\Gamma_\delta(t))$$

$$= -\int_{\Gamma_1}\int_0^1\int_{\mathcal{H}_1(0)\cap(Q_1\cup Q_4)} \epsilon^3|\xi|\partial_S\mathcal{W}^\epsilon(D_e^{\epsilon|\xi|}\boldsymbol{u}^\epsilon \cdot \boldsymbol{e})$$
$$\Delta_{\epsilon\xi}\dot{\boldsymbol{u}}^\epsilon(\boldsymbol{x}) \cdot \boldsymbol{e}\boldsymbol{n} \cdot \boldsymbol{e}\, d\xi\, dr\, dx$$

$$- \int_{\Gamma_2}\int_0^1\int_{\mathcal{H}_1(0)\cap(Q_3\cup Q_4)} \epsilon^3|\xi|\partial_S\mathcal{W}^\epsilon(D_e^{\epsilon|\xi|}\boldsymbol{u}^\epsilon \cdot \boldsymbol{e})$$
$$\Delta_{\epsilon\xi}\dot{\boldsymbol{u}}^\epsilon(\boldsymbol{x}) \cdot \boldsymbol{e}\boldsymbol{n} \cdot \boldsymbol{e}\, d\xi\, dr\, dx$$

$$- \int_{\Gamma_3}\int_0^1\int_{\mathcal{H}_1(0)\cap(Q_2\cup Q_3)} \epsilon^3|\xi|\partial_S\mathcal{W}^\epsilon(D_e^{\epsilon|\xi|}\boldsymbol{u}^\epsilon \cdot \boldsymbol{e})$$
$$\Delta_{\epsilon\xi}\dot{\boldsymbol{u}}^\epsilon(\boldsymbol{x}) \cdot \boldsymbol{e}\boldsymbol{n} \cdot \boldsymbol{e}\, d\xi\, dr\, dx$$

$$- \int_{\Gamma_4}\int_0^1\int_{\mathcal{H}_1(0)\cap(Q_1\cup Q_2)} \epsilon^3|\xi|\partial_S\mathcal{W}^\epsilon(D_e^{\epsilon|\xi|}\boldsymbol{u}^\epsilon \cdot \boldsymbol{e})$$
$$\Delta_{\epsilon\xi}\dot{\boldsymbol{u}}^\epsilon(\boldsymbol{x}) \cdot \boldsymbol{e}\boldsymbol{n} \cdot \boldsymbol{e}\, d\xi\, dr\, dx$$
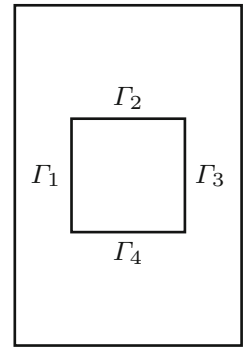$$+ O(\epsilon). \tag{66}$$

When $\boldsymbol{u}^\epsilon \to \boldsymbol{u}^0$ one applies Taylor series to each integrand and passes to the $\epsilon = 0$ limit to get that each integrand in the limit is given by

$$\frac{4|\xi|}{\omega_2}J(|\xi|)h'(0)\mathcal{E}\boldsymbol{u}^0\boldsymbol{e} \cdot \boldsymbol{e}(\dot{\boldsymbol{u}}^0 \cdot \boldsymbol{e})(\boldsymbol{n} \cdot \boldsymbol{e}) \tag{67}$$

so

$$\lim_{\epsilon\to 0} E^\epsilon(\Gamma_\delta(t))$$

$$= -\frac{1}{\omega_2}\int_{\Gamma_1}\int_0^1\int_{\mathcal{H}_1(0)\cap(Q_1\cup Q_4)} 4|\xi|J(|\xi|)h'(0)\mathcal{E}\boldsymbol{u}^0\boldsymbol{e}$$
$$\cdot \boldsymbol{e}(\dot{\boldsymbol{u}}^0 \cdot \boldsymbol{e})(\boldsymbol{n} \cdot \boldsymbol{e})\, d\xi\, dr\, dx$$

$$- \frac{1}{\omega_2}\int_{\Gamma_2}\int_0^1\int_{\mathcal{H}_1(0)\cap(Q_3\cup Q_4)} 4|\xi|J(|\xi|)h'(0)\mathcal{E}\boldsymbol{u}^0\boldsymbol{e}$$
$$\cdot \boldsymbol{e}(\dot{\boldsymbol{u}}^0 \cdot \boldsymbol{e})(\boldsymbol{n} \cdot \boldsymbol{e})\, d\xi\, dr\, dx$$

$$- \frac{1}{\omega_2}\int_{\Gamma_3}\int_0^1\int_{\mathcal{H}_1(0)\cap(Q_2\cup Q_3)} 4|\xi|J(|\xi|)h'(0)\mathcal{E}\boldsymbol{u}^0\boldsymbol{e}$$
$$\cdot \boldsymbol{e}(\dot{\boldsymbol{u}}^0 \cdot \boldsymbol{e})(\boldsymbol{n} \cdot \boldsymbol{e})\, d\xi\, dr\, dx$$

$$- \frac{1}{\omega_2}\int_{\Gamma_4}\int_0^1\int_{\mathcal{H}_1(0)\cap(Q_1\cup Q_2)} 4|\xi|J(|\xi|)h'(0)\mathcal{E}\boldsymbol{u}^0\boldsymbol{e}$$
$$\cdot \boldsymbol{e}(\dot{\boldsymbol{u}}^0 \cdot \boldsymbol{e})(\boldsymbol{n} \cdot \boldsymbol{e})\, d\xi\, dr\, dx. \tag{68}$$

Noting that the integrand has radial symmetry in the ξ variable and (15) (see the calculation below Lemma 6.6 of Lipton (2016)) one obtains

$$\lim_{\epsilon\to 0} E^\epsilon(\Gamma_\delta(t)) = -\sum_{i=1}^4 \frac{1}{2}\int_{\Gamma_i} 2\mathbb{C}\mathcal{E}\boldsymbol{u}^0\boldsymbol{n} \cdot \dot{\boldsymbol{u}}^0\, dx, \tag{69}$$

and (64) follows.

Identical calculations give (37) when we use the contour S_δ and compute the change in energy internal to Q_δ in Fig. 7.

8 Conclusions

It has been shown for the nonlocal model that that the net flux of stress work density through a small contour surrounding the crack is the power per unit length needed to create new fracture surface. This is derived directly from Cauchy's equations of motion for a continuum body (8) (see Sect. 4). In this paper the power balance and kinetic relation given by (27), (28) is not postulated but instead recovered directly from (18) by taking the $\epsilon = 0$ limit. For this case the generalized Irwin relationship is shown to be a consequence of the cohesive dynamics in the $\epsilon = 0$ limit. The recovery is possible since the nonlocal model is well defined

over the failure zone. This suggests that the double well potential of cohesive dynamics provides a phenomenological description of the process zone at mesoscopic length scales. We have illustrated the ideas using the simplest double well energy for a bond based peridynamic formulation. Future investigations will consider state based peridynamic models.

Last we mention that if one fixes the horizon then the ratio r_c to r^+ will affect the size of the process zone hence a brittle to quasi brittle behavior can be expected depending on the ratio. On the other hand for any fixed ratio of r_c to r^+ the process zone goes to zero as the horizon goes to zero and we recover brittle fracture, this is shown theoretically in Lipton (2016). In addition the fracture toughness for the nonlocal model depends on the area underneath the force strain curve and is insensitive to the ratio. This is why this ratio does not show up in the calculations associated with $\epsilon \rightarrow 0$.

References

Atkinson C, Eshelby JD (1968) The flow of energy into the tip of a moving crack. Int J Fract 4:3–8

Anderson TL (2005) Fracture mechanics: fundamentals and applications, 3rd edn. Taylor & Francis, Boca Raton

Bouchbinder E, Goldman T, Fineberg J (2014) The dynamics of rapid fracture: instabilities, nonlinearities and length scales. Rep Prog Phys 77(4):046501

Freund LB (1972) Energy flux into the tip of an extending crack in an elastic solid. J Elast 2:341–349

Freund B (1990) Dynamic fracture mechanics. Cambridge Monographs on Mechanics and Applied Mathematics. Cambridge University Press, Cambridge

Freund B, Clifton RJ (1974) On the uniqueness of plane elastodynamic solutions for running cracks. J Elast 4:293–299

Goldman T, Livne A, Fineberg J (2010) Acquisition of inertia by a moving crack. Phys Rev Lett 104(11):114301

Ha YD, Bobaru F (2010) Studies of dynamic crack propagation and crack branching with peridynamics. Int J Fract 162:229–244

Hu W, Ha YD, Bobaru F, Silling S (2012) The formulation and computation of the nonlocal J-integral in bond-based peridynamics. Int J Fract 176:195–206

Irwin G R (1967) Constant speed, semi-infinite tensile crack opened by a line force. Lehigh University Memorandum

Jha PK, Lipton, (2020) Finite element convergence for state-based peridynamic fracture models. Commun Appl Math Comput 2:93–128

Jha PK, Lipton R (2019b) Numerical convergence of finite difference approximations for state based peridynamic fracture models. Comput Meth Appl Mech Eng 351:184–225. https://doi.org/10.1016/j.cma.2019.03.024

Kostrov BV, Nikitin LV (1970) Some general problems of mechanics of brittle fracture. Arch Mech Stosowanej. 22:749–775

Lipton R (2014) Dynamic brittle fracture as a small horizon limit of peridynamics. J Elast 117(1):21–50

Lipton R (2016) Cohesive dynamics and brittle fracture. J Elast 124(2):143–191

Lipton R, Jha P K (2020). Plane elastodynamic solutions for running cracks as the limit of double well nonlocal dynamics. arXiv:2001.00313

Mott NF (1948) Fracture in mild steel plates. Engineering 165:16–18

Nillison F (1974) A note on the stress singularity at a non-uniformly moving crack tip. J Elast 4:293–299

Ravi-Chandar K (2004) Dynamic fracture. Elsevier, Oxford

Rice JR (1968) A path independent integral and the approximate analysis of strain concentration by notches and cracks. J Appl Mech 9:379–386

Rice JR (1968) Mathematical analysis in the mechanics of fracture. Fracture: An advanced treatise, vol II. Academic Press, New York, p 191

Stenström C, Eriksson K (2019) The J-contour integral in peridynamics via displacements. Int J Fract 216:173–183

Sih GC (1968) Some elastodynamic problems of cracks. Int J Fract Mech 4:51–68

Sih GC (1970) Dynamic aspects of crack propagation. Inelastic Behavior of Solids, McGraw-Hill, pp 607–633

Silling SA (2000) Reformulation of elasticity theory for discontinuities and long-range forces. J Mech Phys Solids 48(1):175–209

Silling SA, Epton M, Weckner O, Xu J, Askari E (2007) Peridynamic states and constitutive modeling. J Elast 88(2):151–184

Silling SA, Lehoucq RB (2010) Peridynamic theory of solid mechanics. Adv Appl Mech 44:73–168

S. A. and Askari, E., (2005) A meshfree method based on the peridynamic model of solid mechanics. Comput Struct 83:1526–1535

Slepian Y (2002) Models and phenomena in fracture mechanics foundations of engineering mechanics. Springer, Berlin

Willis JR (1975) Equations of motion for propagating cracks. The mechanics and physics of fracture. The Metals Society, New York, pp 57–67